ELSEVIER

Journal of Nuclear Materials 250 (1997) 111–117

journal of nuclear materials

Carbon deposition from a γ-irradiated $CO_2/CO/CH_4/C_2H_6$ gas mixture on the manganese oxides MnO, Mn_3O_4 and Mn_2O_3

G.C. Allen *, K.R. Hallam

University of Bristol, Interface Analysis Centre, 121 St. Michael's Hill, Bristol BS2 BBS, UK

Received 12 February 1996; accepted 27 August 1997

Abstract

The composition of oxides formed on steel surfaces within power reactors may influence heat transfer efficiency. Previous studies have indicated that carbon is deposited on spinal-type oxides containing manganese, iron, cobalt, nickel and chromium. In this investigation, characterised manganese oxides have been subjected to γ-irradiation under conditions similar to those experienced in reactors in an effort to understand the catalytic processes involved in deposit initiation and growth. Mn_3O_4 and Mn_2O_3, under the conditions present in the γ-cell, were reduced to MnO during the time of exposure. Relative carbon deposition rates were observed to follow the trend $MnO > Mn_3O_4 \approx Mn_2O_3$. © 1997 Elsevier Science B.V.

1. Introduction

Gas-cooled reactor coolant is based on carbon dioxide, which forms irradiation products capable of attacking the graphite moderator. Degeneration of the moderator may be prevented by the addition of carbon monoxide, methane and water to the coolant. However, an excess of these components may result in the deposition of carbon on fuel cladding and heat-exchanger surfaces, lowering heat transfer efficiency and raising fuel-pin temperatures. Much research has concentrated on the identification of an optimum gas coolant composition to prevent corrosion of the graphite moderator while reducing the rate of carbonaceous deposit on fuel cladding and other surfaces [1].

The temperature of these surfaces varies according to their position in the reactor. Since the composition of the oxide formed on a steel also varies with temperature, a range of oxide compositions would be expected to form on each type of steel. Previous studies [2,3] have shown that nickel–iron or magnetite surfaces catalyse the decomposition of C–H and C–H–O species, such as ethyne or propanone, producing filamentary carbon. The coolant is stable in the absence of radiation but, in reactor, radiolysis of the gas produces several deposition precursors which may be catalytically decomposed to give carbon [4].

The use of isotopically labelled gas mixtures has shown that most of the carbon deposit originates from the methane component of the coolant and that deposition only occurs when this gas is radiolysed [4]. Norfolk et al. [4] have proposed a number of possible pathways leading to the precursor and the following equations represent typical reactions. In the presence of radiation both positive and negative ions may be produced either as single diatomic species or associated with other gaseous atoms or molecules to form a cluster:

$$CO_2 \xrightarrow{h\nu} CO_2^+ + e^-,$$

$$CO \xrightarrow{h\nu} CO^+ + e^-,$$

$$CO_2^+ + nCO_2 \rightarrow (CO_2)_{n+1}^+.$$

The ion clusters can react with hydrocarbons present in the

* Corresponding author. Tel.: +44-117 925 5666; fax: +44-117 9255 646; e-mail: g.c.allen@bristol.ac.uk.

PII S0022-3115(97)00273-0

gas producing a higher hydrocarbon via hydrogen abstraction:

$$CH_4 + (CO_2)_n^+ \rightarrow CH_3^{\cdot} + H(CO_2)_n^+,$$

$$2CH_3^{\cdot} \rightarrow C_2H_6.$$

Higher hydrocarbons can be attacked further to give unsaturated hydrocarbons or hydrocarbon radicals:

$$C_2H_6 + (CO_2)_n^+ \rightarrow C_2H_5^{\cdot} + H(CO_2)_n^+,$$

$$C_2H_5^{\cdot} \rightarrow C_2H_4 + H^{\cdot},$$

$$C_2H_4 + (CO_2)_n^+ \rightarrow C_2H_3^{\cdot} + H(CO_2)_n^+,$$

$$C_2H_4 + H^{\cdot} \rightarrow C_2H_3^{\cdot} + H_2.$$

At gas temperatures below 450–500°C methane destruction produces predominantly C_2H_6 and C_3H_8 with a small proportion being oxidised to carbon monoxide and water:

$$CH_4 + 3CO_2 \rightarrow 4CO + 2H_2O.$$

Above 500°C an increase in both C_2H_4 and the oxidation products CO and H_2O occurs. Previous work has shown that both C_2H_4 production and carbon deposition peak around 550–650°C, supporting the view that C_2H_4 is the main source of deposition. In addition, deposition was shown to be affected to some extent by the presence of CO in the simulated reactor gas and by surface catalysis.

Baker et al. [2] studied the effect of the surface state of iron on carbon deposition and found that FeO was superior to metallic iron as an active catalyst for filamentous carbon formation. Other workers, such as Galuszka and Black [5], found that iron surfaces which had undergone oxidation–reduction treatment decomposed methane to give filamentous carbon, but that untreated iron did not.

In contrast to studies involving iron surfaces, very little has been reported regarding the ability of elements such as manganese to catalyse carbon deposition. Nevertheless, manganese–iron catalysts, which frequently have a surface layer of a spinel-type oxide, are known to be effective for CO decomposition, and the oxidative coupling of methane over manganese oxides has been investigated [6]. Such catalysts produce low molecular mass hydrocarbons in the presence of both CO and hydrogen [7,8], although a carbon deposit can build up on these surfaces reducing their catalytic activity. In an investigation of the behaviour of manganese in surfaces of the spinel series of compounds $Mn_xFe_{1-x}(Fe_2)O_4$, $Mn(Cr_xFe_{2-x})O_4$ and $Mn_xFe_{1-x}(Cr_2)O_4$ it was suggested that Fe^{2+}/Fe^{3+} sites at the surface of these compounds catalysed the formation of dense carbon deposits [9]. However, the role of manganese in these reactions was unclear and to verify the importance of electron transfer in carbon deposition the manganese oxides MnO, Mn_3O_4 and Mn_2O_3 were irradiated under conditions similar to those encountered in a reactor using the γ-cell facility at Magnox Electric's Berkeley Centre.

2. Experimental

2.1. Preparation of samples

The three manganese oxides, MnO (99.5%, green in colour), Mn_3O_4 (99.8%, brown) and Mn_2O_3 (98%, black), used in this study, were obtained from Johnson Matthey, Karlsruhe, as powders. They were pressed into pellets, 8 mm in diameter and 1–2 mm in thickness.

MnO_2 was also investigated. It was characterised by X-ray diffraction and X-ray photoelectron spectroscopy, but it was found impossible to prepare good pellets from this.

2.2. Radiation experiments

Each oxide pellet was loaded into a silica tube with silica spacers designed to allow unimpeded gas flow over the discs. The silica tube was then loaded into a stainless-steel capsule and placed in the γ-cell at Berkeley Centre. A ^{60}Co source is used in this facility. The capsule was placed in an outer irradiation position where a dose rate of 7–9 Gy s^{-1} was obtained [10,11].

2.2.1. Experiment 1: γ-Cell exposure at 550°C

Each oxide was maintained at a temperature of 550°C for 24 days in the γ-cell facility. Gas of composition CO_2–1% CO with 800 vpm (vapour parts per million) CH_4 and 15 vpm C_2H_6 was allowed to flow through the capsule at a rate of 2–3 cm^3 min^{-1} and 40 bar pressure in a single-pass experiment.

2.2.2. Experiment 2: γ-Cell exposure at 650°C

Each oxide was exposed at 650°C for 24 days using the gas composition and flow conditions of experiment 1.

During each experiment, the methane and carbon monoxide concentrations of the capsule inlet and outlet gas were monitored by gas chromatography. From these data, changes in CH_4 and CO concentrations were calculated.

2.3. Energy-dispersive X-ray (EDX) analysis

SEM and EDX analysis was carried out on each sample following exposure using a Cambridge Instruments S150 Mk II fitted with a Kevex windowless detector analysis system. The extent of carbon deposition on each oxide surface was assessed by measuring the carbon-Kα X-ray peak count per 100 s.

2.4. X-ray diffraction (XRD)

XRD spectra were recorded using a Siemens D500 X-ray diffractometer with unfiltered Cu radiation and Siemens Diffrac500 software. A graphite crystal monochromator in the diffracted beam removed Cu K_β fluorescent and incoherently scattered radiation.

2.5. X-ray photoelectron spectroscopy

A Kratos XSAM 800 X-ray photoelectron spectrometer with DS800 software was used for the acquisition and off-line analysis of photoelectron spectra. Measurements were carried out at 1×10^{-9} Torr. The X-ray source was operated at 300 W (20 mA emission current $\times$ 15 kV anode potential).

Samples were mounted on aluminium stubs in holders designed to shield from analysis the outer 0.5 mm of the pellets. This region, when the pellets were mounted for exposure in the gamma cell, was covered by the silica spacers, and thus not exposed to the reactant gases.

Wide scans over the region 0–1000 eV binding energy (BE) were recorded using 20 eV pass energy and 1 eV increments. Narrow regional scans of variable BE range were recorded using the same pass energy and 0.05 eV increments. The wide scans were used to highlight the presence of the main photoelectron peaks in the spectra. All spectra were calibrated against the main peak from the C 1s region at 285 eV.

3. Results

3.1. Gas composition

In these experiments, the increase in CO as the gas passed through the reaction capsule was greater than the reduction in CH_4. One of the reactions occurring in the subcell was the oxidation of the CH_4 to CO and H_2O:

$$CH_4 + 3CO_2 \rightarrow 4CO + 2H_2O.$$

Assuming that the increase in CO which occurred was due solely to this reaction, it is possible to calculate the CH_4 lost by decomposition reactions, such as those described earlier. Both the amount of CO produced by the oxidation reaction and the CH_4 lost by decomposition reactions increased with temperature.

3.2. Optical observations

The manganese oxide pellets after exposure maintained their integrity. Following exposure at both temperatures, the surface of all three oxides was green in colour, indicative of the higher oxidation state pellets being reduced to a common surface chemical composition. When the pellets were split, they were found to be green in their interiors also. Bulk MnO is green in colour, compared to brown Mn_3O_4 and black Mn_2O_3. The reduction process had penetrated the surface to fully reduce the oxides to MnO. The edge regions of the Mn_3O_4 and Mn_2O_3 pellets, shielded from the direct effects of the gas mixture in the gamma cell, were also reduced to MnO.

The MnO pellet exposed within the γ-cell at 550°C had a mottled black surface overlaying its green bulk where the gas mixture came into contact with the pellet. The edges shielded by the spacers were still green. Likewise, the Mn_3O_4 and Mn_2O_3 pellets had green edges surrounding blackened centres. The pellets exposed at 650°C also had darker centres to their faces and green edges, though not as prominent as with the 550°C samples. Both faces of the pellets, that facing the gas inlet end of the capsule and that facing the outlet were of similar appearance. There was no evidence of filamentary or fluffy carbon deposition on any of the samples when examined by scanning electron microscopy. Moreover, no major differences between the appearance of the middle and edges of the pellets was observed.

3.3. Energy dispersive X-ray (EDX) analysis

No impurities were identified in the EDX spectra of the three oxides before exposure. The extent of carbon deposition on each oxide surface facing the gas inlet of the γ-cell was assessed by measuring the carbon-K X-ray peak count per 100 s. Measurements were taken from the central exposed region and the outer edge shielded by the spacers during exposure. Two sets of spectra were recorded at 10 and 20 kV electron beam accelerating voltage. Assuming a density of 2.2 g cm^{-3} for the pressed pellets, electron penetration depths of 0.7 and 3.1 μm were estimated. Table 1 lists the carbon EDX counts for the pellets after exposure. Fig. 1 compares the spectra recorded from the middle and edge of one of the MnO samples after exposure at 550°C.

The MnO pellets showed increased carbon in central regions. The sample exposed at 650°C gave a less intense carbon signal in both the 10 and 20 kV spectra, although, as would be expected, the contribution from the surface carbon was enhanced in the lower energy spectrum, with the shallower average sampling depth. This agreed with the visual observation of the surface being less dark compared to the 550°C pellet.

The results obtained using a 10 kV electron beam accelerating voltage to investigate the Mn_3O_4 pellets also showed some enhancement of the carbon signal, compared to that obtained from the 20 kV spectra. Overall, though,

Table 1
EDX carbon counts (counts $(100\ s)^{-1}$) off the exposed manganese oxides

Sample	C K peak area/counts $(100\ s)^{-1}$							
	550°C				650°C			
	middle		edge		middle		edge	
	20 kV	10 kV	20 kV	10 kV	20 kV	10 kV	20 kV	10 kV
MnO	5801	10 103	2319	3077	2352	4455	1691	2188
Mn_3O_4	2358	3615	-	-	1498	1725	1608	1878
Mn_2O_3	2469	3307	1966	2598	1631	2009	1620	1954

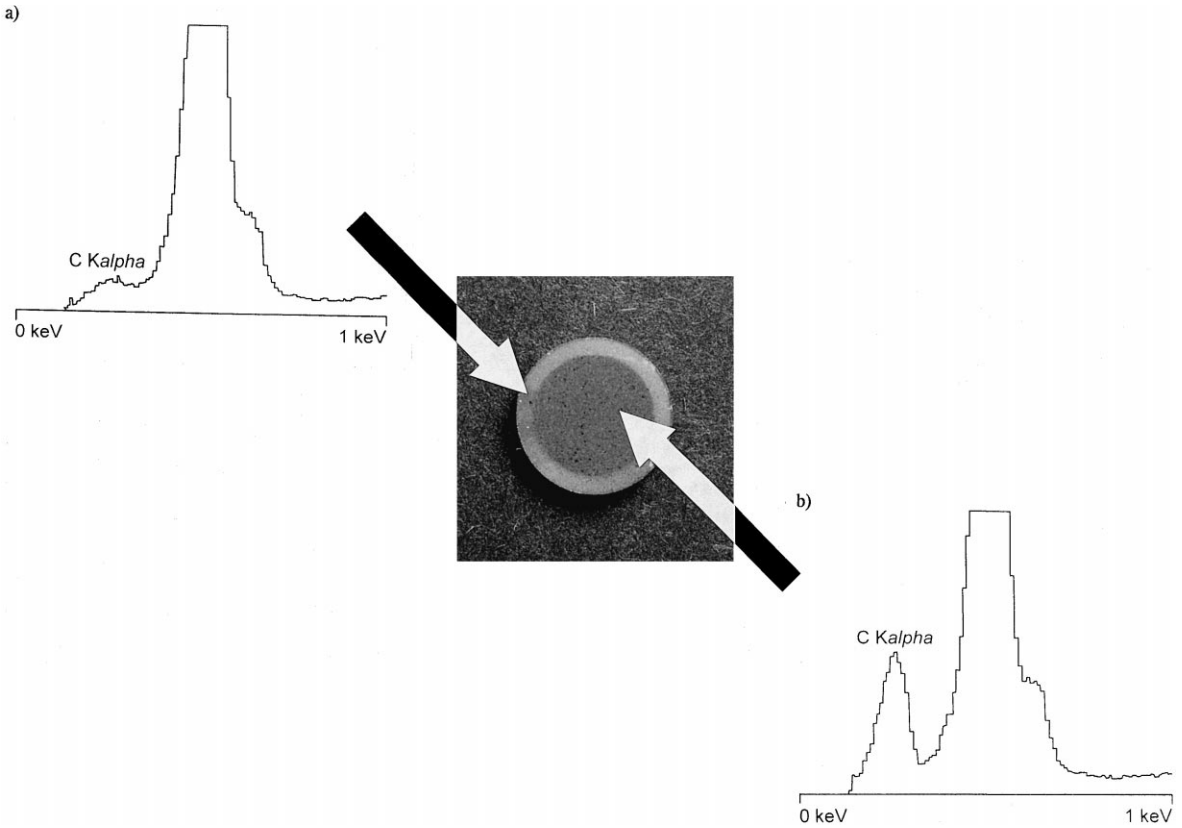

Fig. 1. EDX spectra (carbon region) from (a) edge and (b) middle regions of the MnO pellet after exposure at 550°C.

relatively little deposition was observed on this surface. For Mn_2O_3, greater carbon deposition occurred in central regions of the pellet, particularly following exposure at 550°C, but the signals were less pronounced than those recorded from MnO. Only the MnO pellet produced significant carbon deposition from CO_2–1% CO at both 550 and 650°C. The other oxides, Mn_3O_4 and Mn_2O_3, only appeared to catalyse deposition at 550°C, with similar deposition rates but some $2\frac{1}{2}$ times lower than MnO. The lack of structure in the carbon deposits suggests that a thin film was produced which covered the whole of the exposed pellet surface more or less evenly.

3.4. X-ray diffraction

XRD spectra were recorded from both the oxide powders and pressed pellets prior to γ-cell exposure. There were no differences between the two sets of spectra. The three oxides gave the expected spectra, showing bulk compositions of the correct stoichiometry. All of the pellets, after exposure at both 550 and 650°C, gave only an MnO XRD spectrum, in good agreement with the JCPDS 78-230 manganese oxide/manganosite spectrum and corroborating the visual observations of reduction of the higher oxides down to MnO having occurred, giving the green appearance seen in non-deposited regions of the pellets. No other peaks were seen. Fig. 2 compares the spectra from the Mn_2O_3 pellet before and after exposure at 550°C.

3.5. X-ray photoelectron spectroscopy (XPS)

Table 2 compares the Mn $2p_{3/2}$ binding energies obtained from the oxides before exposure with literature values setting the adventitious C 1s at 285.0 eV [12]. All three samples gave peaks of similar shape and structure. There were no prominent satellite structures observed on the $2p_{3/2}$ and $2p_{1/2}$ peaks.

Table 2 also lists the Mn $2p_{3/2}$ binding energy values obtained from the pellets after exposure in the γ-cell. The Mn_2O_3 and Mn_3O_4 pellets exposed at 550°C gave weak broad Mn $2p_{3/2}$ signals. No signal was recorded from the MnO surface, showing that the layer of deposited carbon completely covered the surface.

Owing to the extent of carbon deposition, information derived from the C 1s XPS results were of limited use. On the oxide samples with high carbon deposition, the carbon layer acted to reduce sample charging by 3–4 eV com-

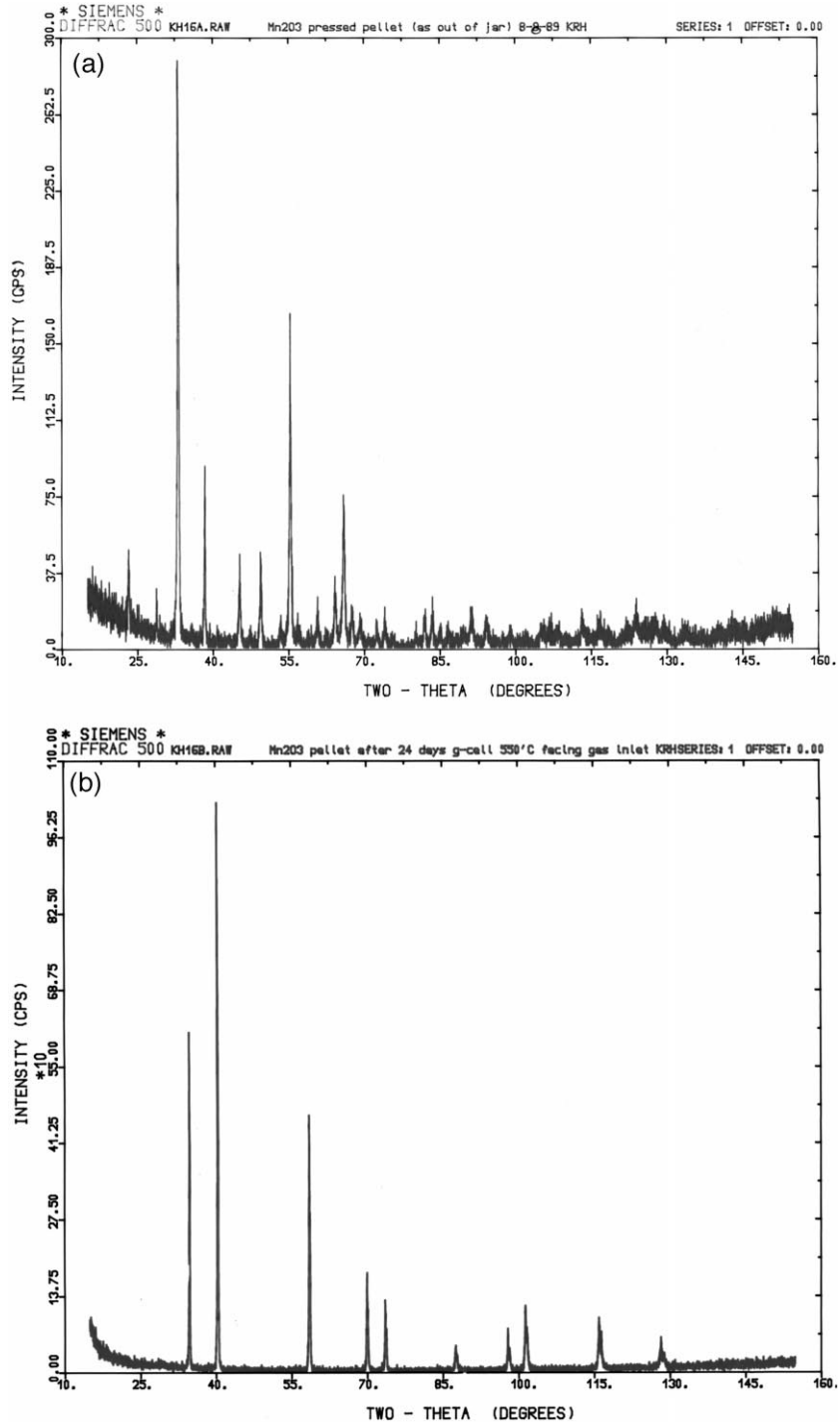

Fig. 2. XRD spectra of an Mn_2O_3 pellet (a) before and (b) after exposure at 550°C.

pared to the minimally deposited Mn_3O_4 and Mn_2O_3 650°C exposed samples. The oxide samples were mounted in aluminium holders to only present the exposed centres of the pellets to analysis. The edges of each sample had been screened from the reactant gases while inside the γ-cell. Therefore, aluminium oxide signals were present in all spectra. This arrangement also contributed additional carbon (and oxygen) signals to the spectra, not necessarily

Table 2
Mn $2p_{3/2}$ binding energy values for the manganese oxides before exposure

Sample	Binding energy (eV)	
	literature value [12]	before exposure
MnO	640.9	640.9
Mn_3O_4	641.4	641.3
Mn_2O_3	641.5	641.6

charged to the same extent as the actual oxide samples themselves, and further detracting from the usefulness of the C 1s results.

4. Discussion

The presence of the Fe^{2+}/Fe^{3+} couple was found to enhance carbon deposition from the gas phase on spinel surfaces. However, Mn_3O_4 unlike magnetite Fe_3O_4, adopts the normal spinel structure in which the Mn^{2+} and Mn^{3+} ions occupy distinguishable sites. Thus, the Mn^{3+} ions are octahedrally coordinated and the Mn^{2+} ions are present only in tetrahedral locations. In Fe_3O_4, both Fe^{2+} and Fe^{3+} are octahedrally coordinated and rapid electron exchange is possible between them at the temperatures involved in this study.

The lack of electron exchange makes Mn_3O_4 a much less intense colour compared to Fe_3O_4 above 120 K [13,14]. If electron exchange in Fe_3O_4 is a cause of carbon deposition, then its absence in Mn_3O_4 would be expected to diminish the extent of deposition on the latter. MnO (Mn^{2+}) and Mn_2O_3 (Mn^{3+}) were chosen to compare the mixed valence oxide, Mn_3O_4, with the corresponding single oxidation state oxides.

X-ray diffraction analysis of the samples after exposure in the gamma cell showed that the Mn_2O_3 and Mn_3O_4 oxides had converted to MnO. This complicates comparisons made between the rates of carbon deposition on the different manganese oxides and of the effect of the presence or absence of the non-interacting Mn^{2+}/Mn^{3+} mixed valency.

None of the samples gave filamentary deposition. Carbon was seen to be deposited on the surfaces in the form of a dense layer, evenly covering the pellet surfaces. The EDX results suggested that MnO was the most effective catalyst of the three manganese oxides examined, and the only one to operate at both temperatures. The other two oxides only catalysed carbon deposition at the lower temperature. Since the MnO pellets gave more carbon deposition than the Mn_3O_4 and Mn_2O_3 ones (which gave roughly similar results), and yet the latter two oxides were, by the end of the exposure, reduced to MnO, it is clear that MnO is a more effective catalyst than either of the other two materials. The time taken for the conversion to MnO was such that the converted pellets probably had insufficient time remaining to accumulate as much deposition as the original MnO samples. In all cases, the MnO carbon deposition was greater than on the other oxides. The Mn_3O_4 did not give large amounts of deposition. The non-interacting Mn^{2+}/Mn^{3+} mixed valency present did not enhance the deposition rate compared to the single valency oxide cases.

MnO has been produced upon exposure of $MnFe_2O_4$ under similar conditions to those used in this work [9]. The MnO produced was thought to be responsible for the increased carbon deposition seen on the manganese ferrite end members of the spinel series $Mn_xFe_{1-x}Fe_2O_4$ and $MnFe_xCr_{2-x}O_4$. In that case, MnO was believed to be acting as a promoter, a role it is known to play in iron containing systems [7,8].

The efficiency of MnO as a carbon coupling catalyst in its own right has been demonstrated to be affected by the gas mixtures used [6]. In CH_4, MnO does not promote the formation of higher hydrocarbons, but Mn_3O_4 does. However, in 50% CH_4/2.5% O_2/47.5% N_2 both oxides were active with MnO showing a conversion rate approximately one third that of Mn_3O_4. (The use of single pulses of gas prevented significant reduction of the Mn_3O_4 to MnO occurring during the time of the experiment.) For the present work, it is significant that MnO in the $CH_4/O_2/N_2$ gas showed a higher selectivity for the formation of C_2 derivatives than did Mn_3O_4 [7]. This indicates that MnO may be more efficient in forming carbon deposits than gas phase products.

The present study has shown that for gas mixtures of the type found in power reactors, MnO is an effective catalyst for the formation of carbon deposits. By contrast, FeO has been shown to be an effective catalyst for the formation of filamentous carbon from hydrocarbons more so than pure iron metal [2,15]. However, the increased catalytic activity is thought to arise not from any intrinsic catalytic capability of the oxide but, instead, from the formation of a high surface area, porous iron structure when the oxide is reduced in the gas conditions present. FeO is a non-stoichiometric compound. It is cation deficient and is usually represented as $Fe_{1-x}O$ in which $x = 0.04–0.12$ [16]. To maintain overall charge neutrality, Fe^{3+} ions are present, in addition to Fe^{2+}. More than 25% of the iron in FeO, wüstite, may be in the 3+ oxidation state. FeO is, therefore, a mixed valence compound, in which the two types of metal ions are located in the same sites. Thus rapid electron exchange is possible between the Fe^{2+} and Fe^{3+} ions. This exchange is expected to play a role in promoting carbon deposition from the gas phase in systems of the type studied here.

MnO, like FeO, is a non-stoichiometric compound. Represented as $Mn_{1-x}O$, where x typically ranges between 0.001 and 0.15 [10,11,15]. Therefore, MnO is a

mixed valence compound, with both Mn^{2+} and Mn^{3+} ions located on the same sites in a rock salt type lattice. As with $Fe_{1-x}O$, there will also be a proportion of the manganese ions located in interstitial sites. Unlike Mn_3O_4, the mixed valency is present on the same lattice, and rapid electron exchange will be possible between the two types of manganese ions with low electron exchange energy as in Fe_3O_4. This type of mixed valency is believed to account for the observation that, of the three manganese oxides studied, MnO gave the greatest extent of carbon deposition upon exposure in the gamma cell.

For the manganese oxides, schemes for the growth of carbon deposits may be suggested as for the mixed valence compound Fe_3O_4. C_2H_4, and the radical formed upon its irradiation C_2H_3, have been shown to be major sources of carbon deposition. Mechanisms for the growth of carbon deposits on the mixed valence $Mn_{1-x}O$ oxide surface can be devised in a manner similar to that for Fe_3O_4 [17]. This involves two possible initiation steps: (1) the formation of a π-bond between $C_2H_3^{\cdot}$ and a Mn^{II}/Mn^{III} site at the surface, through which electron transfer can occur and (2) a σ-bond between a C_2H_3 and an Mn^{II}/Mn^{III} site. Propagation may then proceed via the abstraction of hydrogen atoms from the surface complex by positive ions, such as $CO_2CO_2^+$ present in the irradiated gas mixture. These mechanisms would be expected to leave a catalytic site embedded in the side surface, encouraging the formation of thin, dense deposit layers.

5. Conclusions

For the binary manganese oxides the relative carbon deposition rates were found to follow the order

$$MnO > Mn_3O_4 \approx Mn_2O_3.$$

The non-interacting metal ions present in Mn_3O_4 did not enhance deposition. At both 550 and 650°C, Mn_3O_4 and Mn_2O_3 were reduced to MnO during the time of exposure. The interacting mixed valency present in MnO is believed to enhance carbon deposition in CO_2–1% CO atmospheres.

Acknowledgements

The authors would like to thank Magnox Electric, Berkeley Centre and the Council for National Academic Awards for their support during the course of this work.

References

[1] G.R. Marsh, D.J. Norfolk, R.F. Skinner, CEGB Report TPRD/B/0592/N85, 1985.
[2] R.T.K. Baker, R.J. Alonso, J.A. Dumesic, D.J.C. Yates, J. Catal. 77 (1982) 74.
[3] R.T.K. Baker, J.J. Chludzinski, J. Catal. 64 (1980) 464.
[4] D.J. Norfolk, R.F. Skinner, W.J. Williams, Gas Chemistry in Nuclear Reactors and Large Industrial Plants, Conference Proceedings, University of Salford, UK, April, 1980.
[5] J. Galuszka, M.H. Black, Carbon 22 (1984) 141.
[6] R. Burch, S. Chalker, G.D. Squire, S.C. Tsang, J. Chem. Soc. Faraday Trans. 86 (1990) 1607.
[7] J. Venter, M. Kaminskey, G.L. Geoffroy, M.A. Vannice, J. Catal. 105 (1987) 155.
[8] K.M. Kreitman, B. Baerns, J.B. Butt, J. Catal. 105 (1987) 319.
[9] G.C. Allen, J.A. Jutson, J. Mater. Chem. 1 (1991) 73.
[10] G.C. Allen, J.A. Jutson, J. Chem. Soc. Faraday Trans. 1 (1989) 85.
[11] G.C. Allen, J.A. Jutson, J. Chem. Soc. Faraday Trans. 1 (1989) 55.
[12] J.S. Foord, R.B. Jackman, G.C. Allen, Philos. Mag. A 49 (1984) 657.
[13] M.B. Robin, P. Day, Adv. Inorg. Chem. Radiochem. 10 (1967) 247.
[14] G.C. Allen, N.A. Hush, Prog. Inorg. Chem. 8 (1967) 357.
[15] D.J.C. Yates, J.A. McHenry, Inorg. Chem. 26 (1987) 3193.
[16] G.J. Long, F. Grandjean, Adv. Solid State Chem. 2 (1991) 187.
[17] G.C. Allen, K.R. Hallam, J. Nucl. Mater., 252 (1998) in press.